6872–6882 *Nucleic Acids Research, 2010, Vol. 38, No. 20* *Published online 6 July 2010*
doi:10.1093/nar/gkq506

Long-range effects of histone point mutations on DNA remodeling revealed from computational analyses of SIN-mutant nucleosome structures

Fei Xu, Andrew V. Colasanti, Yun Li and Wilma K. Olson*

Rutgers, the State University of New Jersey, Department of Chemistry and Chemical Biology, BioMaPS Institute for Quantitative Biology, Wright-Rieman Laboratories, 610 Taylor Road, Piscataway, NJ 08854, USA

Received November 14, 2009; Revised May 15, 2010; Accepted May 18, 2010

ABSTRACT

The packaging of DNA into nucleosomes impedes the binding and access of molecules involved in its processing. The SWI/SNF multi-protein assembly, found in yeast, is one of many regulatory factors that stimulate the remodeling of DNA required for its transcription. Amino-acid point mutations in histones H3 or H4 partially bypass the requirement of the SWI/SNF complex in this system. The mechanisms underlying the observed remodeling, however, are difficult to discern from the crystal structures of nucleosomes bearing these so-called SIN (SWI/SNF INdependent) mutations. Here, we report detailed analyses of the conformations and interactions of the histones and DNA in these assemblies. We find that the loss of direct protein–DNA contacts near point-mutation sites, reported previously, is coupled to unexpected additional long-range effects, i.e. loss of intermolecular contacts and accompanying DNA conformational changes at sequentially and spatially distant sites. The SIN mutations seemingly transmit information relevant to DNA binding across the nucleosome. The energetic cost of deforming the DNA to the states found in the SIN-mutant structures helps to distinguish the mutants that show phenotypes in yeast from those that do not. Models incorporating these deformed dimer steps suggest ways that nucleosomal DNA may be remodeled during its biological processing.

INTRODUCTION

DNA wrapped on nucleosomes impedes access to the proteins involved in its biological processing. Moreover, approximately half of the ~147 DNA base pairs wrapped on the surface of the nucleosome face the central core of eight histone proteins. Regulatory factors, such as the SWI/SNF remodeling complex in yeast (*Saccharomyces cerevisiae*), which are recruited by the transcription apparatus, displace the histones and help expose DNA to transcription factors (1,2). How SWI/SNF and other complexes remodel nucleosomes is an area of active investigation (3–7).

Point mutations of the genes that code for histones H3 and H4 can relieve the requirement of the SWI/SNF complex in yeast-screening experiments (8). A number of point mutations—including R116H and T118I in H3 and V43I, R45H and R45C in H4—can restore the viability of yeast cells in the absence of the SWI/SNF complex. The biochemical properties of nucleosomes bearing any one of these so-called SIN (SWI/SNF INdependent) mutations differ in many ways from the wild-type nucleosome (3,4,9). How these mutations might alter the transcription of nucleosome-bound DNA in yeast is not clear from the known X-ray structures (9,10). The assembly of protein and DNA in the five available SIN-mutant nucleosome core-particle structures shows only minimal distortions from the wild-type structure around the mutation sites (9), i.e. a few contacts lost from protein to DNA, and the overall global folding appears to be the same.

Four other nucleosome structures that contain alanine mutants where the four key amino-acid residues normally occur (R116 and T118 in H3, V43 and R45 in H4) also resemble the wild-type structure, as do two other

*To whom correspondence should be addressed. Tel: +1 732 445 3993; Fax: +1 732 445 5958; Email: wilma.olson@rutgers.edu
Present addresses:
Fei Xu, Department of Biochemistry, University of Medicine and Dentistry of New Jersey, Center for Advanced Biotechnology and Medicine, Piscataway, NJ 08854, USA.
Andrew V. Colasanti, Rutgers, the State University of New Jersey, Department of Chemistry & Chemical Biology, NJ 08854, USA.
Yun Li, Chemistry and Biochemistry Department, Delaware Valley College, Doylestown, PA 18501, USA.

nucleosome structures, where the cationic R45 in H4 is replaced by an anionic glutamic acid (R45E) and where T118 in H3 is replaced by a more bulky and potentially positively charged histidine (T118H). Except for the crystal structures, very little is known about the biochemical properties of these six mutant nucleosomes or their potential effects on yeast-screening experiments.

The SIN-mutant nucleosome structures share the same DNA sequence but contain different pairs of mutant histones, i.e. single point mutations in both copies of H3 or H4. These mutations are clustered near the dyad of the nucleosome at superhelical location (SHL) ± 0.5, i.e. roughly half a helical turn on either side of the symmetry axis of the structure (10). DNA wraps around the SIN-mutant nucleosomes along a left-handed pathway similar to that formed by the corresponding molecules in the wild-type structure (10–12), with the loss of a few minor-groove contacts at the mutation sites (9).

This paper presents a detailed analysis of the differences in DNA structure and histone–DNA interactions in the SIN-mutant nucleosome structures compared to the wild type. The analysis includes (i) the number of close histone–DNA contacts lost or gained upon the mutation of H3 or H4 in the complete assembly, (ii) the accompanying conformational changes in DNA, (iii) the cost of deforming the DNA to these states and (iv) the simulated remodeling of DNA based on this information. These analyses reveal unexpected long-range effects of SIN mutations, i.e. conformational changes and loss of contacts to the histone proteins at sites on DNA that are sequentially and spatially distant from the mutation sites. Models, which incorporate these highly deformed steps, are suggestive of ways that nucleosomal DNA may be remodeled during its biological processing.

METHODS

Contacts of protein to DNA atoms

The distances between atoms in the wild-type and SIN-mutant nucleosome structures are calculated using an algorithm, which assigns atoms to a $5\,\text{Å} \times 5\,\text{Å} \times 5\,\text{Å}$ cubic grid and scans only atom pairs within each grid or between neighboring grids. This algorithm reduces the computational complexity from the order of N^2 for an exhaustive pairwise distance calculation to the order of N. Here, the contacts of protein to DNA atoms are limited to values within a specified cutoff distance (taken to lie between 3.2 and 4.0 Å, at increments of 0.2 Å).

The number of amino-acid residues at the N- and C-termini of the histone subunits in the different crystal structures varies. Only the residues common to both the wild type and all of the SIN-mutant structures are counted in the tabulation of histone–DNA contacts (Supplementary Figure S1).

Base-pair-step parameters and remodeling

Six independent base-pair-step parameters termed Shift, Slide, Rise (three translations) and Tilt, Roll, Twist (three rotations) uniquely define the relative position and orientation of two successive base pairs (13). These six parameters are computed with the 3DNA software package (14–16), which uses the standard reference frame established by the nucleic-acid structural biology community (17) and a rigorous, matrix-based algorithm (18–20). With the same algorithm and standard reference frame, the nucleosome structures can be rebuilt from the values of the 'step' parameters with the 3DNA software. Moreover, because the software allows the user to place the global coordinate frame on any base-pair step, one can easily determine the effects of isolated conformational changes on the folding of nucleosomal DNA and identify structural pathways potentially taken in remodeling the nucleosome.

Color-coding

We generate color-coded dot plots to visualize the differences in both the number of contacts and the values of step parameters in the SIN-mutant structures compared to the wild-type nucleosome. We divide a given range of values $[-t,t]$ of these differences into 21 intervals and assign a color to a base pair or base-pair step along the DNA—one of 21 shades of blue, gray or red—based upon the magnitude x of the parameter at that site. Any value that lies outside the specified range, i.e. $x < -t$ or $x > t$, will be color-coded with the darkest blue or red, respectively. Intermediate values of the parameter are assigned an interval number i and color based upon interpolation:

$$i = \begin{cases} 1 & x < -t \\ \left[11.5 + \frac{x}{v}\right] & -t \le x \le t \\ 21 & x > t \end{cases} \quad (1)$$

Here v is the length of the interval, equal to $t/10$, and the square parentheses designate the integer closest to that obtained from the formula. The colors change from blue to gray to red with increase in i. In order to draw attention to the major structural differences between the SIN-mutant and wild-type nucleosomes, values of x associated with any of the central 11 intervals are assigned the same shade of gray.

Threading

The threading score measures the ease of deforming a DNA sequence along the three-dimensional pathway found in a high-resolution structure (21,22). The pathway is defined by the set of base-pair-step parameters characterizing the DNA in the selected structure. Here, we consider DNA scaffolds of variable lengths taken from the wild-type and SIN-mutant nucleosome crystal structures. The scaffolds range between 60 and 130 bp steps in length, with the structural dyad (the 73rd base pair in these 146-bp structures) lying in all cases at the center of the template. Thus, scaffolds of 60 bp steps encompass the interactions of the two copies of histones H3 and H4 with nucleosomal DNA, and templates of 130 bp steps include almost all of the interactions between DNA and the histone octamer (two copies of H2A, H2B, H3 and H4). The DNA sequences crystallized in the wild-type and SIN-mutant nucleosome structures differ slightly

(see Figure S2 in the Supplementary Data). We thread both sequences on 96 structural templates, i.e. eight different scaffolds (60, 70,. . ., 130-bp steps in length) from each of 12 nucleosome structures. The Protein Data Bank (23) and Nucleic Acid Database (24) identifiers of the structures (PDB and NDB IDs) are listed in the Supplementary Data (Table S1).

The cost of deforming each base-pair step from its preferred equilibrium state to the three-dimensional arrangement found on the structural template is calculated with a knowledge-based function (25) derived from the observed configurations (step parameters) of consecutive base pairs of the same sequence in other (non-nucleosomal) protein–DNA complexes. The sum of the deformation scores of each base-pair step in a given reading frame, or setting, along the nucleosomal DNA sequence is collected and referred to as the threading score. The data plotted in Figure 1 depict the cost of threading all 86 possible 61-bp fragments from the 146-bp α-satellite DNA sequence crystallized in the wild-type nucleosome structure, 1 bp at a time, on the central 61 bp (60-bp steps) of that structure. The different settings of the sequence on the template [Figure 1(a)] change the identities of the base pairs constrained to specific structural arrangements. The threading scores vary because the cost of specific base-pair-step deformations depends upon sequence (see below).

The threading score E of an N+1 bp (N bp step) nucleosomal DNA sequence in the i—th reading frame on a structural template of L bp steps is expressed in terms of the six base-pair-step parameters as

$$E_i = \sum_{n=i}^{i+L-1} \left(\frac{1}{2} \sum_{j=1}^{6} \sum_{k=1}^{6} f_{jk}(\mathrm{MN}) \Delta\theta_j^n \Delta\theta_k^n \right). \quad (2)$$

Here $\Delta\theta_j^n = \theta_j^n - \theta_j^0(\mathrm{MN})$ is the deviation imposed by the structural template on the j—th step parameter θ_j^n at base pair n from the equilibrium rest state $\theta_j^0(\mathrm{MN})$ characteristic of the MN dimer, and the $f_{jk}(\mathrm{MN})$ are stiffness constants associated with the MN step (25). The threading index i spans the range $i = 1, \ldots, N-L+1$ and the step parameter identities $j = 1,6$ correspond respectively to Shift, Slide, Rise, Tilt, Roll and Twist. The values of $\theta_j^0(\mathrm{MN})$ are the average values of the base-pair-step parameters in a large data set of protein-bound DNA molecules (other than nucleosomes) (22), and the $f_{jk}(\mathrm{MN})$ are extracted from the pairwise covariance of these data. The composite function is thought to reflect the natural conformational characteristics of the base-pair steps (25). Given that all energy terms are positive, the threading score will increase with the length L of the structural template.

RESULTS

Protein–DNA contacts in the SIN-mutants versus the wild-type nucleosome

Although the SIN-mutants closely resemble the wild-type nucleosome at the global level, the structures show subtle

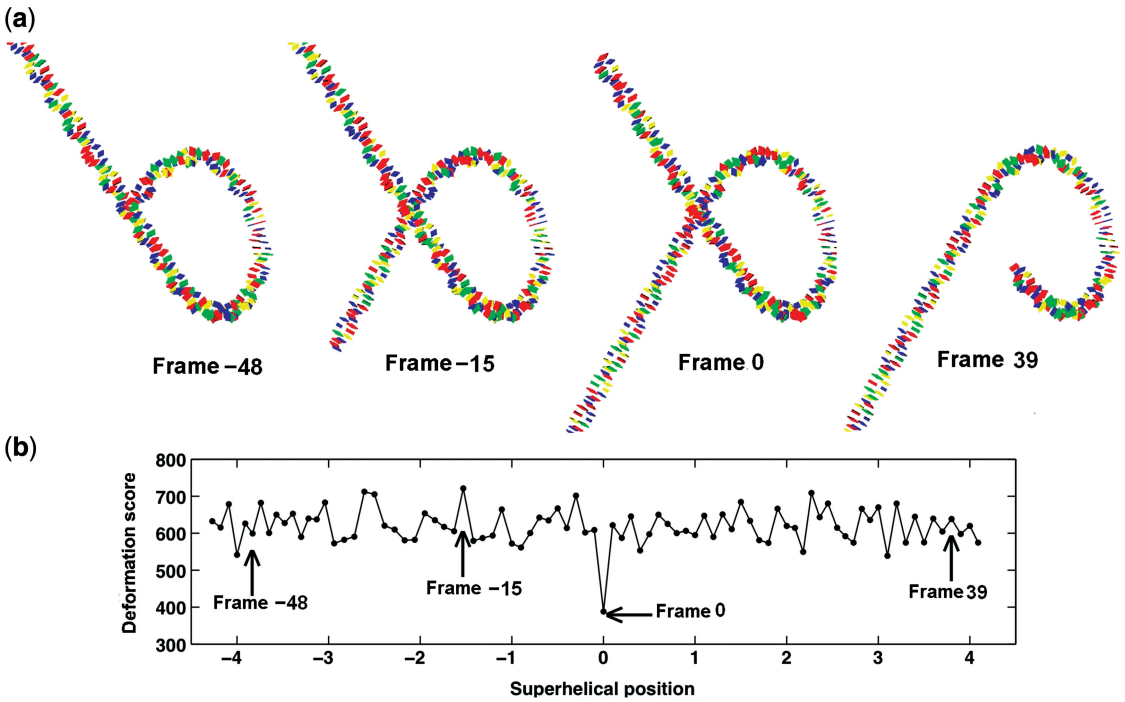

Figure 1. Schematic diagram of the threading of DNA on a virtual nucleosome template. (**a**) Snapshots of four settings of a 146-bp nucleosomal DNA sequence from the wild-type structure on a 60-bp-step nucleosomal template centered at the dyad of the same structure. The DNA slides 1 bp at a time along the three-dimensional template. The frame numbers (−48, −15, 0 and 39) denote the dinucleotides that lie on the central step of the template in each setting and correspond to the distances of those dimers, in base-pair steps, from the natural (observed) setting of the sequence on the dyad of the crystal structure. (**b**) Deformation score, computed with [Equation (2)], of each reading frame versus superhelical position along the nucleosomal DNA. The arrows below the threading scores denote the reading frames/settings shown in (a). Frame 0 corresponds to the sequence in its natural setting.

differences in local contacts and conformations. For example, the SIN mutants contain on average ~10% fewer DNA–histone contacts than the wild-type structure. There are 228 close inter-atomic contacts (separated by distances of 3.4 Å or less) between DNA and protein in the wild-type structure. The average number of contacts lost over all the SIN-mutant structures is 23.5 at this cutoff. One of the five SIN-mutant structures, which shows the phenotype in yeast-screening experiments, has a smaller contact loss of 17.

Surprisingly, although the SIN mutations occur in the center of the bound DNA near superhelical position SHL ±0.5, the sites of contact loss are scattered along the 146-bp duplex. The contact losses noted previously in the vicinity of the SIN mutations (9) account for roughly a quarter of the total loss of atomic interactions. Other contacts disappear at sites one or two helical turns away, i.e. SHL −1.5 and −2.5, in the majority of SIN-mutant structures (Figure 2). There is also a significant contact loss near the two ends of the DNA, i.e. at SHL ±5.5, locations sequentially and spatially even further away from the mutation sites. In some SIN-mutants, contact losses occur at SHL ±1 and −4.4. The contact losses at a number of points, e.g. SHL ±5.5, occur in concert with large changes in the B factors of DNA and the displacement of both DNA and protein relative to the wild-type structure (Figures S4 and S5 in the Supplementary Data). The protein found at these sites, however, remains stiff in terms of the measured B factors. Despite the potential ambiguity in the positions of the DNA atoms, the patterns of contact loss persist at different cutoffs (3.2–4.0 Å) (Supplementary Figure S6), suggesting that the observed contact losses may not be related entirely to the uncertainty of the crystal structures, but at least in part to real differences in the protein–DNA interactions.

DNA deformations in the SIN-mutants compared to the wild-type nucleosome

The contact losses in the SIN-mutant nucleosomes tend to be accompanied by deformations of the DNA base-pair steps compared to those in the wild-type structure. There are noticeable changes in Slide, a conformational parameter that describes the displacement of successive base pairs along their long axes and the accompanying dislocation of the helical axis, as well as in Roll and Tilt, the two components of local DNA bending. The changes in these three base-pair-step parameters occur near the sites of SIN mutations, i.e. the central region of the nucleosome at SHL ± 0.5, as well as at more distant sites, including the ends of the bound DNA (SHL ±1.5, ±2.5, ±4-6) (Figure 3). There are no corresponding patterns of conformational change and no large jumps in the remaining step parameters (Twist, Shift and Rise), which are thus not shown.

Although there are no large global conformational changes in the DNA bound to the SIN-mutant nucleosomes compared to the wild-type structure, the local

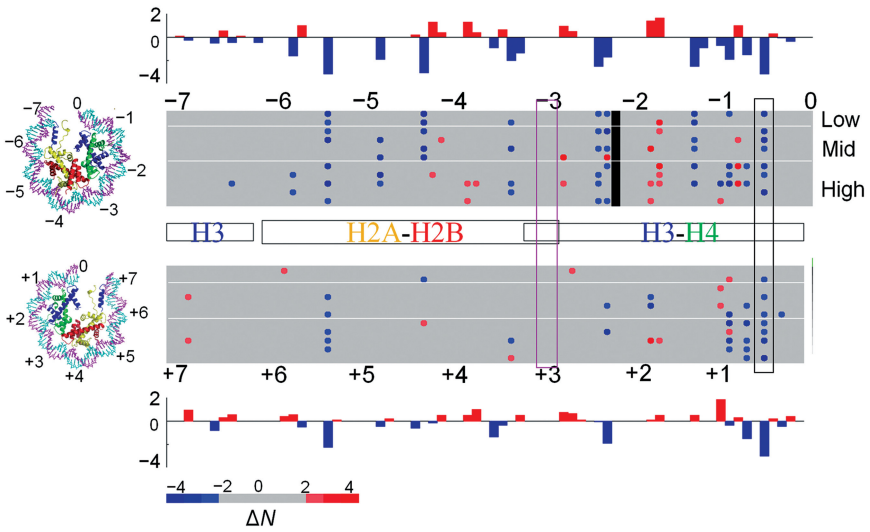

Figure 2. Difference in the numbers of close (≤3.4 Å) interatomic contacts between histone protein cores and DNA atoms in SIN-mutant nucleosome structures compared with the wild-type. Data, mapped at each nucleotide along the DNA, show the short- and long-range effects of the SIN mutations. The two pseudo-symmetrical halves of nucleosomal DNA, whose 3D representations are on the left of the diagram, are represented by two 'blocks' with superhelical positions (from –7 to +7) corresponding to the DNA sites labeled in the 3D images. Average gain or loss of contacts in each SIN-mutant structure compared to the wild type is plotted in the histograms at the top and bottom of the figure. White horizontal lines within the blocks divide the eleven structures into three groups (Low, Mid and High) according to the threading scores shown in Figure 4: (top) low-scoring group—R116A and V43I; (middle) mid-scoring group—V43A, R116H, R45E and T118A; (bottom) high-scoring group—T118H, R45C, T118I, R45H and R45A. The dimerization interface between histones H3–H4 and H2A–H2B, and the sequential locations of SIN mutations are highlighted respectively by the magenta- and black-edged vertical windows. The relative locations of histone proteins with respect to DNA are indicated by the three horizontal blocks in the middle of the diagram (the small block labeled H3 represents the histone-tails in contact with the ends of the DNA). A 'phantom' base-pair step (the black square in each row of the upper block) is inserted at position −21 to maximize the alignment of contact differences in the two halves of the DNA. The difference in the number of contacts (ΔN) of the mutants versus the wild type is shown in different shades of blue (negative) and red (positive). Differences of −2 to +2 are shown in gray. See color-coded scales at the bottom of the figure, and refer to Figure S3 in the Supplementary Data for the numbers and locations of close contacts in the wild-type structure.

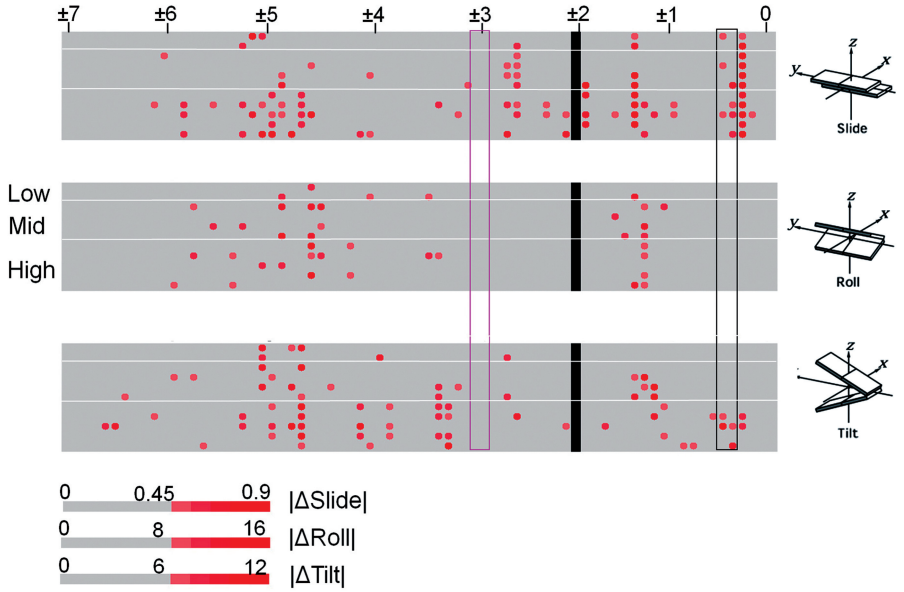

Figure 3. Differences in the step parameters that describe the arrangements of successive base pairs in SIN-mutant nucleosome structures compared with the wild-type, mapped on each base-pair step of DNA. The 'block' images on the right illustrate the step parameters of interest, the values of which are obtained with the 3DNA software package (14–16). Data reported here are averages of the absolute values of the differences in the parameters over the two halves of each structure, i.e. the magnitude of the change in a given base-pair-step parameter at a specific dinucleotide in the first half (dimer steps −73 to −1), and the magnitude of its pseudo-symmetrical counterpart in the second half (dimer steps +1 to +73). The differences, compared to the wild type, in the step parameters in each half of the structures are shown in Supplementary Figure S7. Note that there is no dimer step 0 and that superhelical location 0 at the top of the figure is a point dividing the structures into two 73-dimer-step halves, i.e. the first half includes the 'phantom' dinucleotide step used in Figure 2 to 'symmetrize' the 146-bp DNA structure. Data are color-coded in shades of red, with smaller variations in step parameters depicted in gray. The color-coded range of |ΔSlide|, the difference in the shearing displacement of successive base pairs along their long axes, is set to be three times the standard deviation $\sigma_{|\Delta\text{Slide}|}$ of the values of |ΔSlide| in all SIN-mutant structures, i.e. $3\sigma_{|\Delta\text{Slide}|} = 0.9$ Å. The color-coded ranges of |ΔRoll| and |ΔTilt|, the differences in the bending components, are four times the corresponding standard deviations. See color-coded scales at the bottom of the figure. Structures are presented in the same order as in Figure 2.

variations of Slide, Roll and Tilt are significant in terms of the mean values and dispersion of data found from statistical studies of the base-pair-step parameters in other protein–DNA complexes (22). The Slide differs from the wild-type value by as much as 1.7 Å in some SIN mutants, a value comparable to the change of Slide that accompanies the transformation of double-helical DNA from the B form to the A or C forms (14). The differences of Roll and Tilt also far exceed the usual variation of values in protein-bound DNA complexes, i.e. ΔRoll values as large as 18°, twice the standard deviation of Roll, and ΔTilt values as large as 16°, five times the standard deviation of Tilt (22,25). Although the relatively low resolution (2.3–3.0 Å) of the SIN-mutant structures introduces uncertainty in atomic-level information, such as the identities of DNA and protein atoms within specific contact limits (see above), the positions of the electron densities of the bases are clear in even the most poorly resolved nucleosome structures. Hence, the step parameters deduced from the positions of the bases provide one of the most reliable measures of the deformation of DNA in the various molecular assemblies.

Threading

The accumulated distortions of local base-pair geometry lead to appreciable differences in the cost [Equation (2)] of wrapping DNA around the SIN-mutant histone cores compared to the corresponding protein assembly in the wild-type nucleosome. The deformation scores of DNA sequences forced to adopt the configurations found in the SIN-mutant nucleosomes consistently exceed the scores associated with the wild-type structure (Figure 4). The 146-bp DNA sequence crystallized in the presence of the mutant histone cores differs at two positions compared to that found in the wild-type structure. The thymine located at base pair −3 and the adenine found at base pair +4 in the wild-type assembly are replaced respectively by guanine and cytosine in all the SIN-mutant structures (Supplementary Figure S2). Despite these differences, the threading scores of the two sequences on the same structural template, i.e. specific three-dimensional pathway, are similar (see Figure 4 for the scores of the wild-type sequence on various nucleosome scaffolds and Supplementary Figure S5 for those of the modified DNA sequence on the same structures).

The scores reported here correspond to the cost of threading DNA fragments of increasing lengths (60-130-bp steps) on the 'natural' settings of different nucleosome structures, e.g. the 61 bp in the center of the crystallized sequence on the central 60-bp steps of the structure. The cost of deforming the DNA in other structural settings is substantially higher, as previously reported (21), for shortened fragments of the 147-bp human α-satellite DNA found in the currently best-resolved nucleosome core-particle structure (26) (also see Figure 1 in the 'Methods' section where the

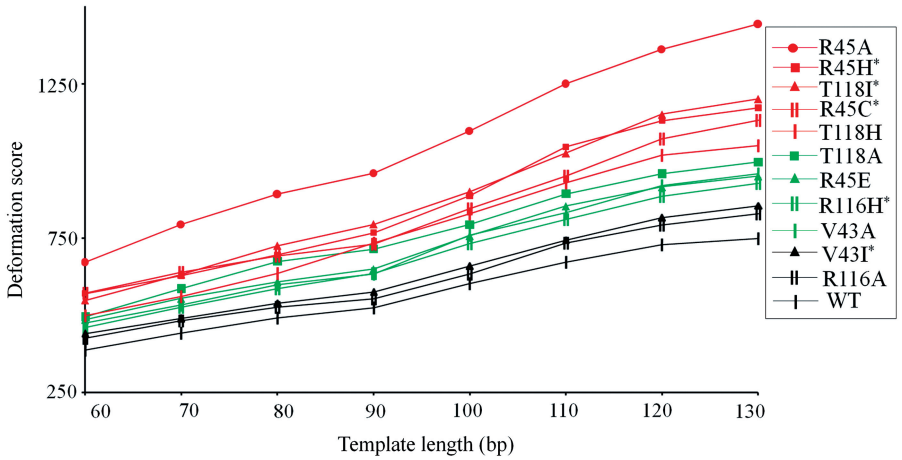

Figure 4. Threading scores of the wild-type DNA sequence in its 'natural' setting on different structural templates of variable length. The templates are extracted from the wild-type (WT) and SIN-mutant nucleosome structures, whose identities are shown at the right. The SIN mutants with phenotypes that relieve dependency on the SWI/SNF complex in yeast-screening experiments are labeled with an asterisk. All templates are centered at the structural dyad. For example, the 100-bp-step template spans the central 101 bp of the nucleosome structure with 50 symmetrically related dimers on either side of base pair 0 on the dyad.

'natural' lowest-scoring setting of a 61-bp DNA sequence is located at superhelical position 0 and the cost of threading the same sequence in any other setting is ~50% higher in value). The precise setting, however, does not affect the relative threading scores on the various SIN-mutant structures, i.e. a particular structural template occupies the same relative scoring position whether the DNA is threaded in the 'natural' lowest-scoring setting or allowed to sample all possible settings on that structure (compare Figure 4 versus Supplementary Figure S9).

The threading scores on the SIN-mutant structures fall into three distinct groups (Figure 4): a high-scoring group (H3 T118H, H4 R45C, H3 T118I, H4 R45H, H4 R45A), which includes three of the SIN-mutant nucleosomes (here underlined) showing the phenotype in yeast; an intermediate-scoring group (H4 V43A, H3 R116H, H4 R45E, H3 T118A) with one of the phenotypic nucleosomes; and a low-scoring group with the wild-type (WT) and one of the phenotypic nucleosomes (H3 R116A, H4 V43I). The same grouping trends persist with structural templates of different lengths, with different sequence settings (described above), and with the modified DNA sequence in place of the wild type (Supplementary Figure S8).

Simulated DNA remodeling

The subtle differences in the wrapping of DNA on the SIN-mutant nucleosomes compared to the wild-type structure suggest ways in which the histone point mutations might 'remodel' DNA and thereby relieve the need for the SWI/SNF remodeling complex in yeast-screening experiments (8). Here, we illustrate the potential effects of the most costly deformations of local DNA conformation found in the H4 R45H SIN-mutant structure on the folding of DNA around the wild-type nucleosome. The selected deformations contribute to the high cost of threading DNA on the H4 R45H complex. This nucleosome not only forms the best-resolved (2.3 Å) SIN-mutant crystal structure and introduces some of the most costly deformations of DNA around the histone core, but also functions independently of the SWI/SNF complex in yeast-screening experiments (8). Although the DNA wrapped on the H4 R45A mutant is more highly deformed than that on the H4 R45H structure, the nucleotides that code for arginine preclude the occurrence of an alanine point mutation in yeast-screening experiments, i.e. it is impossible to transform any of the arginine codons to an alanine codon via a single nucleotide mutation. On the other hand, the high-scoring H4 R45A mutant, created by recombinant protein expression and crystallized as a structural control (9), lowers the barrier to temperature-induced nucleosome repositioning, ('sliding') in much the same way as the H4 R45 SIN mutants expressed in yeast, and as shown in Supplementary Table S2 the deformations of DNA base-pair steps in the H4 R45A structure closely resemble those in the H4 R45H complex.

We 'remodel' the wild-type nucleosome by introducing the base-pair-step geometry that seemingly contributes to the high deformation scores of DNA on the H4 R45H SIN-mutant structure. The most costly base-pair steps cluster in three distinct regions of the complex (Figure 5 and Supplementary Table S2), namely the two ends of the bound DNA (steps −55, −52, −51 between SHL −5.5 and −5, steps +41 and +48 between SHL +4 and +4.8) and a duplex fragment over a helical turn away from the sites of SIN mutations (steps −20, −15, −14, −13 between SHL −2 and −1.5). We replace the DNA wrapped around the wild-type structure by various combinations of these 'high-energy' steps and superimpose the remodeled structures (cyan) on the wild-type (gray) DNA pathway (Figure 6). Although these isolated conformational moves may be sterically forbidden (in that parts of the DNA may clash with the assumed rigid histone interior), their effect on DNA folding is suggestive of the changes that might occur during the remodeling process.

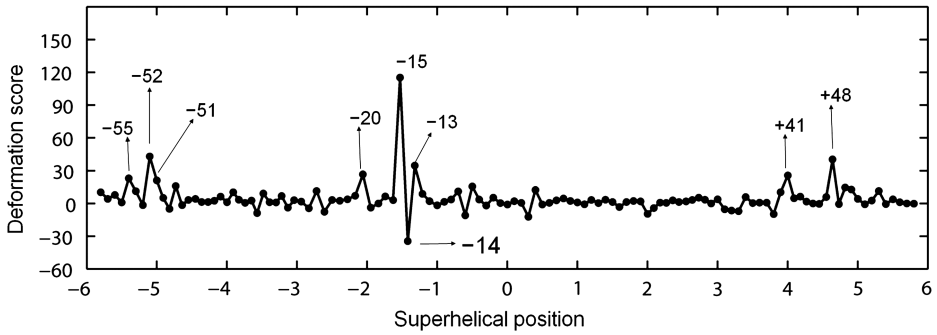

Figure 5. The difference of deformation energy scores of the wild-type DNA sequence threaded on the central 120-bp steps of the H4 R45H SIN-mutant structure compared to the corresponding wild-type template. Base-pair steps are denoted by their superhelical positions (−5.8 to +5.8). Dimer steps, where the absolute values of the difference of deformation scores are 20 or higher, are labeled with the step numbers.

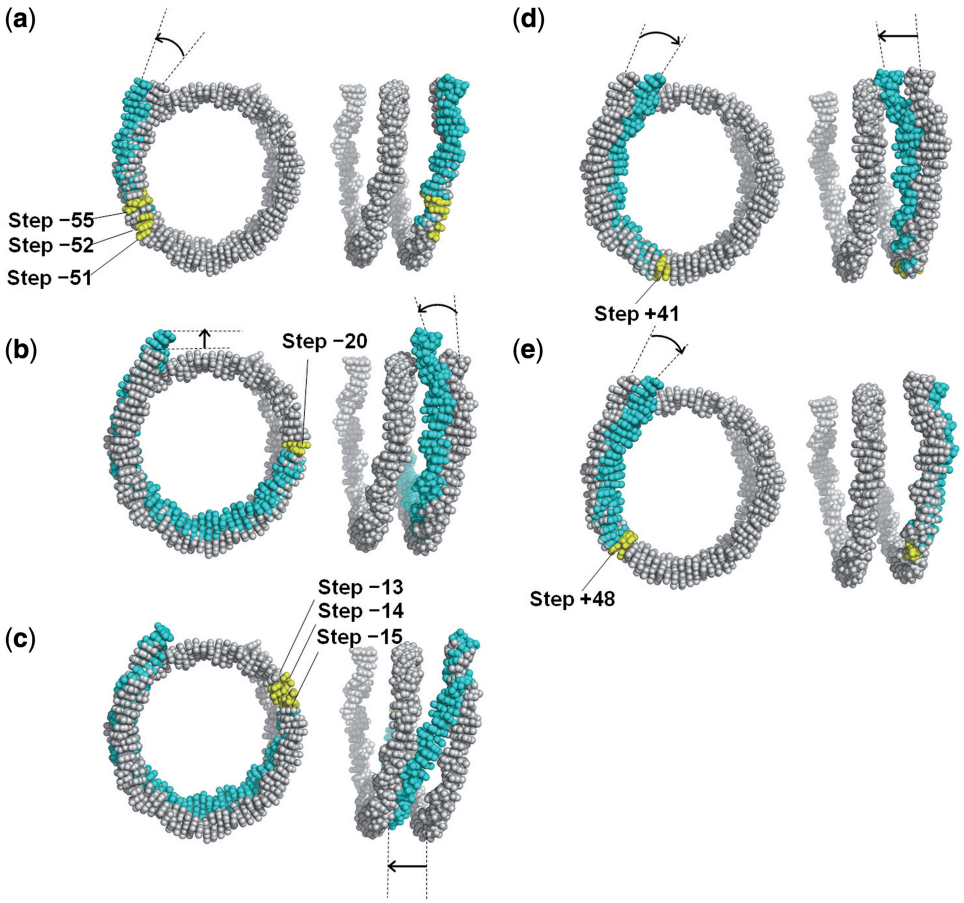

Figure 6. Top and side views of the wild-type nucleosome structure 'remodeled' in five different ways on the basis of the values of the five largest differences in local threading scores on the H4 R45H SIN-mutant template compared to the wild-type (differences of 20 or higher). The steps from the wild-type structure are replaced by selected steps from the H4 R45H structure: (**a**) steps −55, −52 and −51, (**b**) step −20, (**c**) steps −13, −14 and −15, (**d**) step +41 and (**e**) step +48. Remodeled and wild-type structures are superimposed on the central base pair. The wild-type DNA and the part of the remodeled DNA, which overlaps the wild-type, are shown in gray. The altered pathway of the remodeled DNA is shown in cyan. The dimer steps with altered parameters are highlighted in yellow and labeled. As dimer steps +41 and +48 are located in the second half of the nucleosomal DNA, the viewpoints are flipped 180° about the vertical axis through the dyads in (d, e) compared to those in (a–c) so as to show the remodeled pathway from the same perspective. See also Figure 5.

The presence of the 'high-energy' base-pair steps changes the wrapping and/or pitch of DNA on the nucleosome. For example, the introduction of the three deformed steps found at the 5′-end of the H4 R45H structure peels DNA off and away from the modeled nucleosome [Figure 6(a)]. By contrast, the remodeling of base-pair step −20 at SHL −2 decreases the superhelical pitch and directs the 5′-end of the DNA away from the

protein core [Figure 6(b)]. Concomitant remodeling of the DNA at base-pair steps −15 to −13 has an even more pronounced effect on the superhelical pitch of DNA [Figure 6(c)], and the perturbations found at base-pair steps +41 at SHL +4 or +48 at SHL +4.8 make the 3′-end of the chain swing inward [Figure 6(d) and (e)]. Notably, the same types of double-helical rearrangements, i.e. DNA unpeeling and changes in pitch, occur if the wild-type nucleosome is 'remodeled' using the high-energy steps from other less well-resolved nucleosome structures. Moreover, some of these isolated changes, although quite different in detail from those presented here, affect the overall DNA fold in much the same way.

The combined uptake of the nine most highly deformed steps from the H4 R45H structure in the wild-type nucleosome introduces all of the above changes in global structure while concomitantly producing an asymmetry in the DNA pathway (Supplementary Figure S10). The tighter superhelical turn of the 5′-end of the modeled DNA precludes normal binding to the histone assembly and suggests possible disruption of the protein core.

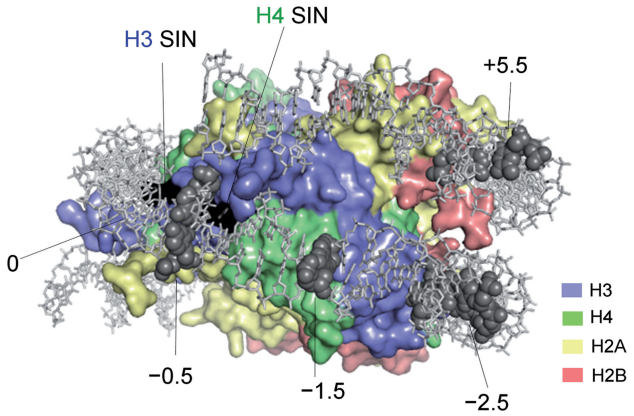

Figure 7. A side view of the wild-type nucleosome core-particle structure highlighting the locations of SIN mutations and the regions of contact loss in mutant structures compared to the wild type. The histone subunits are color-coded by protein type: blue (H3); green (H4); yellow (H2A); and red (H2B). The SIN mutation sites are emphasized in black on the left side of the protein surface. The two strands of DNA are shown as light gray 'sticks'. The base pairs bearing contact loss at superhelical positions −2.5, −1.5, −0.5 and +5.5 (base-pair positions −23/−22, −13, −5 and +55, respectively) are represented by dark gray spheres and labeled by their superhelical positions.

DISCUSSION

Long-range changes in DNA structure

Although the SIN-mutant nucleosome structures closely resemble all other known nucleosome structures at the global level, our detailed analyses show numerous contact losses and accompanying large conformational changes scattered along the DNA, including major distortions of double-helical structure at sites which are far away from the locations of the SIN mutations. These long-range structural changes may reflect allosteric interactions involving the histone proteins. Loops at the ends of two long α-helices, one from H3 and the other from H4, bind in the vicinity of the SIN mutation sites (SHL ±0.5). Loops at the other ends of the same α-helices bind DNA about two double-helical turns away at SHL ±2.5. The differences in DNA conformation at the SIN-mutation sites appear to be transmitted along these long α-helices (see the blue and green α-helices in the top-down views of the nucleosome in Figure 2).

The H3–H4 histone dimer, bound to the central region of one half of the nucleosome, e.g. SHL 0 to −3 in the first half of the structure, stacks against the H2A-H2B dimer bound to the end region of the other half of the complex, e.g. SHL +4 to +7 in the second half. A 'side' view of the nucleosome (Figure 7), perpendicular to the superhelical axis, shows that two sites of major protein–DNA contact loss in the SIN-mutants, at SHL +5.5 and SHL −2.5, lie directly above each other (Figure 7). The apparent allosteric interactions of histone H3-H4 and H2A-H2B dimers between SHL ±0.5 and ±2.5 appear to be further transmitted through space in the SIN-mutants from SHL −2.5 to +5.5. Although there is a corresponding loss of contacts at SHL −5.5, there is no accompanying loss of contacts at SHL +2.5, suggesting that a different mechanism may be in place in the other half of the structure. The latter difference might be related to the known asymmetry of the SIN-mutant nucleosome structures, with unequal lengths of DNA (72 and 73 bp) bound to the two halves. As is well known, the DNA is over stretched between SHL −1.5 to −2.5 in the 72-bp half of the 146-bp structure (10).

DNA unwrapping and protein invasion

Interestingly, the strongest resistance to DNA unzipping (strand separation) found in recent single-molecule experiments, occurs around the dyad and in the end regions of the nucleosome from SHL ±5 to ±4 (27). These sites correspond to locations (SHL ±0.5, −4.9 and −4.5; Figures 2 and 3) where contact loss and large conformational changes occur in the SIN-mutants compared to the wild-type structure. Thus, the DNA might be unzipped more easily from the histone proteins in SIN-mutant nucleosomes in similar single-molecule strand-separation experiments. The contact loss at SHL ±5.5 is not accompanied by any significant conformational changes in the SIN-mutant structures. Possibly both contacts and conformational change are needed for the unzipping response.

The interactions of various protein assemblies—RNA polymerase II (28,29), RSC [a complex for remodeling the structure of chromatin (30)] (4,7), and SWI/SNF (4)—with nucleosomes induce the dissociation of the H2A–H2B dimer. The same type of contact loss found at the end regions bound to H2A–H2B in the SIN-mutant structures might contribute to this behavior. The correspondence between the extent to which these proteins invade the nucleosome (SHL −5.5, −4.5) (28,29) and the sites of contact loss reported here (SHL −4.9, −4.5, −5.5; Figure 2) suggests that the contact losses might not be artifacts of the crystal structures.

The contact loss at SHL −1.5 and the accompanying conformational changes in Slide and Roll at nearby

base-pair steps lie only 10 bp, or one helical turn, away from the SIN-mutation sites. As is well known, the conformation of nucleosomal DNA differs significantly in the region SHL −1.5 to −2 in the 72-bp half of a 146-bp nucleosome compared to that in its 'symmetric' counterpart between SHL +1.5 and +2 in the 73-bp half. The minor groove of the wild-type structure is narrower and the Twist is greater at position −1.5 compared to position +1.5 (31). The root-mean-square deviation of corresponding atoms is also higher at these sites than in any other parts of the bound DNA (10). As noted by others (31,32), these differences may be related to the packing of crystals, since the stacking between the 73- and 72-bp halves of neighboring nucleosomes in the crystal lattice is a major driving force of crystallization. The greater distances of the arginine side groups (H3 R63) from the exposed minor-groove edges of the bases at position −1.5 (33) further suggests that this region might be more flexible than other bound parts of the DNA. The structural response of the 146-bp nucleosomal DNA to SIN mutations presumably reflects these same effects. That is, the intrinic asymmetry and deformability of the site leads to more pronounced changes in DNA conformation and greater loss of contact with protein at SHL −1.5 versus +1.5.

Deformation scores and simulated remodeling

The local deformations of nucleosomal DNA help to distinguish the SIN-mutant structures that show phenotypes from those that do not. The deformation scores tend to be higher and the local conformational changes greater for the SIN-mutant structures that are found to be independent of the SWI/SNF remodeling complex in yeast-screening experiments. Moreover, three out of the five SIN-mutants in the high-scoring group—H4 R45C, H3 T118I and H4 R45H—translocate easily on nucleosomal DNA in biochemical studies (6,9). Only two SIN-mutants with phenotypes in yeast have lower deformation energies, H3 R116H in the intermediate-scoring group and H4 V43I in the low-scoring group. Consistently, these two mutants show less remodeling capabilities than the SIN-mutants with the phenotype in the high-scoring group (6,9). Furthermore, the high deformation score of the DNA in H4 R45A construct, a histone mutant precluded by codon constraints in conventional genetic-screening experiments, suggests that that a mutant of this type, produced through genetic engineering, may relieve the requirement of the SWI/SNF nucleosome remodeling complex in yeast. Like the SIN-mutant nucleosomes found to function in the absence of the SWI/SNF assembly, the H4 R45A nucleosome also shows a strong tendency to translocate along DNA (9).

Simulated remodeling of nucleosomal DNA from knowledge of the strongest deformation steps in the SIN-mutant structures hints of how histone proteins may come on and off or reorient the nucleosome core particle in the absence of remodeling proteins such as the SWI/SNF complex. Substitution of the DNA structure in the wild-type nucleosome by the costly moves seen in the SIN-mutant structures results in two kinds of global changes. In one type, the end regions flex, i.e. the first half stretches out and the second half swings in. This same kind of opening might be related to the dissociation of H2A–H2B during ATP-dependent nucleosome remodeling (4) and might facilitate the invasion of the transcription machinery (28,29). The model resembles the spontaneous peeling of DNA off the histone core seen in recent time-lapse atomic-force microscopic measurements (34) and detected with various other techniques, e.g. site-exposure protein-binding equilibria (35) and single-molecule fluorescence measurements (36–38). Moves of this type may also explain why the H4 R45H mutant is more accessible to micrococcal nuclease than the wild-type nucleosome (3). H4 R45H has high remodeling capabilities (6,9). Yeast cells bearing H4 R45H show higher resistance to ultraviolet (UV) damage due to a higher DNA-repairing capability, which might be related in turn to the ease of unwrapping of DNA off the nucleosome (39).

The second type of global move is a change in pitch associated with a so-called 'kink-and-slide' conformation (21) at one of the minor-groove binding sites. Step −15 (the GG:CC dimer at SHL −1.5) with a large positive Slide (1.9 Å) and negative Roll (−57.2°) in the H4 R45H SIN-mutant structure, is highly deformed compared to the corresponding step in the wild-type structure (Slide = 0.32 Å, and Roll = −31.2°) (Supplementary Table S2). Simulated remodeling shows that this step dramatically decreases the superhelical pitch. Similar pitch-controlling steps with the same types of 'kink-and-slide' arrangements occur at steps ±17 (the AG:CT dimer at SHL ±1.5) in the 147-bp nucleosome structure (PDB ID: 1KX5) (26). The diminished pitch in the simulated remodeling also suggests a local conformational pathway responsible for the chiral rearrangements of DNA, i.e. transitions between left- and right-handed superhelical folds, detected in the $(H3–H4)_2$ tetramer–DNA particle (40,41).

Finally, the 'remodeling' of DNA described in this work is highly simplified, with no corrections made for steric hindrance. The models, nevertheless, reveal general conformational trends consistent with what little is known about the likely deformations of nucleosomal DNA. The costly base-pair steps, which are unique to the SIN-mutant nucleosome structures, may contribute to the remodeling of DNA in the absence of the SWI/SNF protein assembly. Our primitive findings reveal the need for more detailed structural and computational studies of nucleosomal DNA rearrangements. The simple constructs of 'melted' nucleosomes that we have built can be easily generated by others using our 3DNA software tools (14–16) and then taken as a starting point for elaborate atomic-level studies.

SUPPLEMENTARY DATA

Supplementary Data are available at NAR online.

ACKNOWLEDGEMENTS

The authors would like to thank Dr. Karolin Luger for introducing us to this project and for sharing the

coordinates of nucleosome structures in advance of publication and Dr. Xiang-Jun Lu for encouraging the development of our color-coded conformational-analysis tools and for providing valuable technical assistance with the 3DNA software package.

FUNDING

The U.S. Public Health Service under research grants GM20861 and GM34809 and instrumentation grant RR022375. Partial funding for open access change: U.S.P.H.S. grant GM3409.

Conflict of interest statement. None declared.

REFERENCES

1. Alberts,B., Johnson,A., Lewis,J., Raff,M., Roberts,K. and Walter,P. (2002) *Molecular Biology of the Cell*, 4th edn, Chapter 4. Garland Publishing, New York.
2. Lewin,J. (2004) *Genes VIII,* Chapter23. Pearson Prentice Hall, Upper Saddle River, NJ.
3. Kurumizaka,H. and Wolffe,A.P. (1997) Sin mutations of histone H3: influence on nucleosome core structure and function. *Mol. Cell. Biol.*, **17**, 6953–6969.
4. Bruno,M., Flaus,A., Stockdale,C., Rencurel,C., Ferreira,H. and Owen-Hughes,T. (2003) Histone H2A/H2B dimer exchange by ATP-dependent chromatin remodeling activities. *Mol. Cell*, **12**, 1599–1606.
5. Flaus,A. and Owen-Hughes,T. (2003) Mechanisms for nucleosome mobilization. *Biopolymers*, **68**, 563–578.
6. Flaus,A., Rencurel,C., Ferreira,H., Wiechens,N. and Owen-Hughes,T. (2004) *Sin* mutations alter inherent nucleosome mobility. *EMBO J.*, **23**, 343–353.
7. Carey,M., Li,B. and Workman,J.L. (2006) RSC exploits histone acetylation to abrogate the nucleosomal block to RNA polymerase II elongation. *Mol. Cell*, **24**, 481–487.
8. Kruger,W., Peterson,C.L., Sil,A., Coburn,C., Arents,G., Moudrianakis,E.N. and Herskowitz,I. (1995) Amino acid substitutions in the structured domains of histones H3 and H4 partially relieve the requirement of the yeast SWI/SNF complex for transcription. *Genes Dev.*, **9**, 2770–2779.
9. Muthurajan,U.M., Bao,Y., Forsberg,L.J., Edayathumangalam,R.S., Dyer,P.N., White,C.L. and Luger,K. (2004) Crystal structures of histone Sin mutant nucleosomes reveal altered protein-DNA interactions. *EMBO J.*, **23**, 260–271.
10. Luger,K., Mäder,A.W., Richmond,R.K., Sargent,D.F. and Richmond,T.J. (1997) Crystal structure of the nucleosome core particle at 2.8 Å resolution. *Nature*, **389**, 251–260.
11. Arents,G. and Moudrianakis,E.N. (1993) Topography of the histone octamer surface: repeating structural motifs utilized in the docking of nucleosomal DNA. *Proc. Natl Acad. Sci. USA*, **90**, 10489–10493.
12. Ramakrishnan,V. (1997) Histone structure and the organization of the nucleosome. *Annu. Rev. Biophys. Biomol. Struct.*, **26**, 83–112.
13. Dickerson,R.E., Bansal,M., Calladine,C.R., Diekmann,S., Hunter,W.N., Kennard,O., von Kitzing,E., Lavery,R., Nelson,H.C.M., Olson,W.K. *et al.* (1989) Definitions and nomenclature of nucleic acid structure components. *Nucleic Acids Res.*, **17**, 1797–1803.
14. Lu,X.-J. and Olson,W.K. (2003) 3DNA: a software package for the analysis, rebuilding and visualization of three-dimensional nucleic acid structures. *Nucleic Acids Res.*, **31**, 5108–5121.
15. Lu,X.-J. and Olson,W.K. (2008) 3DNA: a versatile, integrated software system for the analysis, rebuilding and visulization of three-dimensional nucleic-acid structures. *Nat. Protoc.*, **37**, 1213–1227.
16. Zheng,G., Lu,X.-J. and Olson,W.K. (2009) Web 3DNA-a web server for the analysis, reconstruction, and visualization of three-dimensional nucleic-acid structures. *Nucleic Acids Res.*, **37**, W240–W246.
17. Olson,W.K., Bansal,M., Burley,S.K., Dickerson,R.E., Gerstein,M., Harvey,S.C., Heinemann,U., Lu,X.-J., Neidle,S., Shakked,Z. *et al.* (2001) A standard reference frame for the description of nucleic acid base-pair geometry. *J. Mol. Biol.*, **313**, 229–237.
18. Zhurkin,V.B., Lysov,Y.P. and Ivanov,V.I. (1979) Anisotropic flexibility of DNA and the nucleosomal structure. *Nucleic Acids Res.*, **6**, 1081–1096.
19. Bolshoy,A., McNamara,P., Harrington,R.E. and Trifonov,E.N. (1991) Curved DNA without A-A: experimental estimation of all 16 DNA wedge angles. *Proc. Natl Acad. Sci. USA*, **88**, 2312–2316.
20. El Hassan,M.A. and Calladine,C.R. (1995) The assessment of the geometry of dinucleotide steps in double-helical DNA; a new local calculation scheme. *J. Mol. Biol.*, **251**, 648–664.
21. Tolstorukov,M.Y., Colasanti,A.V., McCandlish,D., Olson,W.K. and Zhurkin,V.B. (2007) A novel roll-and-slide mechanism of DNA folding in chromatin: implications for nucleosome positioning. *J. Mol. Biol.*, **371**, 725–738.
22. Balasubramanian,S., Xu,F. and Olson,W.K. (2009) DNA sequence-directed organization of chromatin: structure-based computational analysis of nucleosome-binding sequences. *Biophys. J.*, **96**, 2245–2260.
23. Berman,H.M., Westbrook,J., Feng,Z., Gilliland,G., Bhat,T.N., Weissig,H., Shindyalov,I.N. and Bourne,P.E. (2000) The Protein Data Bank. *Nucleic Acids. Res.*, **28**, 235–242.
24. Berman,H.M., Olson,W.K., Beveridge,D.L., Westbrook,J., Gelbin,A., Demeny,T., Hsieh,S.-H., Srinivasan,A.R. and Schneider,B. (1992) The Nucleic Acid Database. A comprehensive relational database of three-dimensional structures of nucleic acids. *Biophys. J.*, **63**, 751–759.
25. Olson,W.K., Gorin,A.A., Lu,X.-J., Hock,L.M. and Zhurkin,V.B. (1998) DNA sequence-dependent deformability deduced from protein-DNA crystal complexes. *Proc. Natl Acad. Sci. USA*, **95**, 11163–11168.
26. Davey,C.A., Sargent,D.F., Luger,K., Maeder,A.W. and Richmond,T.J. (2002) Solvent mediated interactions in the structure of the nucleosome core particle at 1.9 Å resolution. *J. Mol. Biol.*, **319**, 1097–1113.
27. Hall,M.A., Shundrovsky,A., Bai,L., Fulbright,R.M., Lis,J.T. and Wang,M.D. (2009) High-resolution dynamic mapping of histone-DNA interactions in a nucleosome. *Nat. Struct. Mol. Biol.*, **16**, 124–129.
28. Kireeva,M.L., Walter,W., Tchernajenko,V., Bondarenko,V., Kashlev,M. and Studitsky,V.M. (2002) Nucleosome remodeling induced by RNA polymerase II: loss of the H2A/H2B dimer during transcription. *Mol. Cell*, **9**, 541–552.
29. Kireeva,M.L., Hancock,B., Cremona,G.H., Walter,W., Studitsky,V.M. and Kashlev,M. (2005) Nature of the nucleosome barrier to RNA polymerase II. *Mol. Cell*, **18**, 97–108.
30. Cairns,B.R., Lorch,Y., Li,Y., Zhang,M., Lacomis,L., Erdjument-Bromage,H., Tempst,P., Du,J., Laurent,B. and Kornberg,R.D. (1996) RSC, an essential, abundant chromatin-remodeling complex. *Cell*, **87**, 1249–1260.
31. Suto,R.K., Edayathumangalam,R.S., White,C.L., Melander,C., Gottesfeld,J.M., Dervan,P.B. and Luger,K. (2003) Crystal structures of nucleosome core particles in complex with minor groove DNA-binding ligands. *J. Mol. Biol.*, **326**, 371–380.
32. White,C.L., Suto,R.K. and Luger,K. (2001) Structure of the yeast nucleosome core particle reveals fundamental changes in internucleosome interactions. *EMBO J.*, **20**, 5207–5218.
33. Rohs,R., West,S.M., Sosinsky,A., Liu,P., Mann,R.S. and Honig,B. (2009) The role of DNA shape in protein–DNA recognition. *Nature*, **461**, 1248–1253.
34. Shlyahhtenko,L.S., Lushnikov,A.Y. and Lyubchenko,Y.L. (2009) Dynamics of nucleosomes revealed by time-lapse atomic force microscopy. *Biochemistry*, **48**, 7842–7848.
35. Widom,J. (2001) Role of DNA sequence in nucleosome stability and dynamics. *Quart. Rev. Biophys.*, **34**, 269–324.
36. White,C.L. and Luger,K. (2004) Defined structural changes occur in a nucleosome upon Amt1 transcription factor binding. *J. Mol. Biol.*, **342**, 1391–1402.

37. Li,G., Levitus,M., Bustamante,C. and Widom,J. (2005) Rapid spontaneous accessibility of nucleosomal DNA. *Nat. Struct. Mol. Biol.*, **12**, 46–53.
38. Kelbauskas,L., Chan,N., Bash,R., DeBartolo,P., Sun,J., Woodbury,N. and Lohr,D. (2008) Sequence-dependent variations associated with H2A/H2B depletion of nucleosomes. *Biophys. J.*, **94**, 147–158.
39. Nag,R., Gong,F., Fahy,D. and Smerdon,M.J. (2008) A single amino acid change in histone H4 enhances UV survival and DNA repair in yeast. *Nucleic Acids Res.*, **36**, 3857–3866.
40. Hamiche,A., Carot,V., Alilat,M., De Lucia,F., O'Donohue,M.-F., Revet,B. and Prunell,A. (1996) Interaction of the histone $(H3\text{-}H4)_2$ tetramer of the nucleosome with positively supercoiled DNA minicircles: potenial flipping of the protein from a left- to a right-handed superhelical form. *Proc. Natl Acad. Sci. USA*, **93**, 7588–7593.
41. Alilat,M., Sivolob,A., Revet,B. and Prunell,A. (1999) Nucleosome dynamics IV. protein and DNA contributions in the chiral transition of the tetrasome, the histone (H3-H4)2 tetramer-DNA particle. *J. Mol. Biol.*, **291**, 815–841.